Thermo-mechanical analysis of fire effects on the structural performance of shield tunnels

Citation for published version:
Shen, Y, Zhu, H, Yan, Z, Zhou, L, Zhang, T, Men, Y & Lu, Y 2023, 'Thermo-mechanical analysis of fire effects on the structural performance of shield tunnels', *Tunnelling and Underground Space Technology*, vol. 132, 104885, pp. 1-13. https://doi.org/10.1016/j.tust.2022.104885

Digital Object Identifier (DOI):
10.1016/j.tust.2022.104885

Link:
Link to publication record in Edinburgh Research Explorer

Document Version:
Peer reviewed version

Published In:
Tunnelling and Underground Space Technology

Thermo-mechanical analysis of fire effects on the structural performance of shield tunnels

Yi Shen [a,b,c], Hehua Zhu [a,b], Zhiguo Yan [a,b*], Long Zhou [b], Tong Zhang [b], Yanqing Men [d],

Yong Lu[c]

[a] *State Key Laboratory of Disaster Reduction in Civil Engineering, Tongji University, 1239 Siping Road, Shanghai 200092, China*

[b] *Department of Geotechnical Engineering, College of Civil Engineering, Tongji University, 1239 Siping Road, Shanghai 200092, China*

[c] *Institute for Infrastructure and Environment, School of Engineering, The University of Edinburgh, Edinburgh EH9 3JL, UK*

[d] *Jinan Rail Transit Group Co., Ltd, Jinan 250101, China*

Abstract: Investigating fire effects is a continuing endeavour in the research and practice communities concerned with the design and safety of shield tunnels. This paper aims to provide a comprehensive model for the assessment of structural safety of a shield tunnel segmental ring exposed to fire. A thermo-mechanical model for assembled shield tunnel structure in fire is developed to provide a basis for a holistic analysis by incorporating tunnel lining segments and longitudinal joints, as well as improved predictions for the temperature, stress and deformation distributions in the tunnel structure. Validation of the numerical results against experimental data shows satisfactory agreement. Parametric studies are subsequently conducted to investigate the effects of spalling, buried depth and cooling-off phases on the fire behaviour of the shield tunnel. The results show that the damage and failure of a tunnel lining structure under high temperature are mainly due to the combined action of internal thermal expansion force and thermal stress. Spalling leads to the loss of a key “insulation” layer of a tunnel lining structure. On the other hand, the constraint of strata on the tunnel structure under high temperature not only restrains the deformation of key parts of the structure, but also helps offset the adverse effect of load on the structure through elastic resistance.

Keywords: Fire effect; Shield tunnel; Thermo-mechanical model; Structural performance; Numerical analysis

1. Introduction

Fire is an important subject for a wide range of design, operation and maintenance processes of tunnels. Many historical fire incidents have confirmed that, while tunnel fires may not necessarily cause the collapse of a tunnel structure, significant damage can occur to the tunnel lining, and such damage in turn can result in long-term disruption to traffic or rail services leading to major economic losses (Carvel, 2019; Casse and Caroly, 2019; Hua et al., 2021; Ren et al., 2019; Zhang et al, 2021a; b). For instance, in 2001 two trucks crashed and this triggered a fire and induced serious structural damage at the Gotthard Road Tunnel in Switzerland (Chen et al., 2013). In 2008, a heavy goods vehicle fire lasted for around 16 hours resulting in severe damage of tunnel structure in the Channel Tunnel in France (Beard and Carvel, 2011). In 2015, a fire induced by a gasoline tank truck sparked fast spread of fire over 500 m and the tunnel structure was severely damaged in the Skatestraum Tunnel in Norway (Zhang et al., 2021). In all these historical fire incidents, severe spalling of concrete was observed and this directly exposed one or more layers of reinforcement to high temperatures. Despite the numerous fire incidents causing tunnel damage, however, there is still a lack of generally accepted approach to analysing these complex systems for a quantitative performance assessment that enables fire safety engineers to establish, in an explicit manner, an adequate fire safety strategy. As the provision of fire resistance is not a design objective or criterion in most transportation infrastructure standards, the fire resistance of tunnel structures is generally lower than that in buildings (Kodur and Naser, 2020).

Previous research studies have mainly focused on the fire performance of isolated members of shield tunnel. On the experimental side, various studies have been conducted to support grading evaluations and analysis of structural safety of lining structures in fire (Du et al., 2018; Qiao et al., 2019; Tomar and Khurana, 2019; Yan et al., 2012; 2015; 2016; 2020; Zhang et al, 2021c; e). Only a small number of experimental studies have been carried out on a whole tunnel structure setting in fire due to high costs. Yan et al. (2013) conducted experiments on small scale shield tunnel lining structures for metro tunnels to investigate the thermo-mechanical behaviour and fire damage under different load conditions. Ring et al. (2014) carried out fire tests and numerical analysis on concrete frame structures simulating tunnel structures and described the temperature field distribution across the sections of the structural members, the deformation at different positions and the concrete bursting. Alhawat et al. (2021) conducted large-scale fire exposure testing of two unloaded tunnel rings in the RABT fire curve. These experiments to some extent demonstrated the deformation behavior of the entire structure, but the experimental conditions were restricted and the monitoring data were limited.

On the other hand, the numerical simulation has been adopted by many researchers, using simplified modelling methods such as a layered beam model or detailed finite element (FE) analysis. Detailed finite element analysis has been used to carry out comprehensive simulation of the mechanical behaviour of the continuous tunnel rings under fire, and calculate the corresponding bearing capacity and fire resistance time (Choi et al., 2013; Chang, 2016; Colombo et al., 2015; Lilliu and Meda, 2013). By combining the method of fluid dynamics and multiphase porous media mechanics, Bergmeister et al. (2020) simulated the mechanical response of the arched tunnel structure under fire. Ouyang et al. (2021) employed the FE method to examine the flexural response of drop ceiling panels in rock tunnels to several fire curves. Although it has been recognised that the mechanical properties of joints is a key that could dictate the structural performance and integrity of shield tunnels (Shen et al., 2021), previous numerical simulations of shield tunnel structures have generally been conducted without regard to the presence of joints and hence could not represent the realistic mechanical behaviour of segmental rings, especially in terms of the integrity and stability of the overall tunnel structure.

In all, much has been accomplished from the experimental and numerical studies in terms of understanding the general behaviour of shield tunnel structures in fire. However, few studies have attempted to investigate the shield tunnel structure with discontinuous joints. On the other hand, limited information is available with regard to the parametric influences on the performance of segmental lining structures in fire.

In this paper, a holistic analysis approach is developed for the nonlinear structural analysis and design of the segmental tunnel rings incorporating lining segments and longitudinal joints, as well as an improved transient thermal analysis. The accuracy of the numerical model is verified by comparing the analysis results with the data from previous fire experiments involving complex nonlinear behaviour of the tunnel structural members. Based on the parametric calculations using the proposed model, the influences of spalling, buried depth and cooling-off phase on the temperature distribution, structural deformations and mechanism of failure are discussed. The proposed analysis framework enables the analysis of whole tunnel rings in fire in a practical calculation environment, and the parametric results should inform the development of improved fire resistance provisions in design codes and retrofitting strategies for upgrading fire-damaged shield tunnels.

2. Modelling approach

An finite element (FE) approach is employed to evaluate the response of loaded and restrained reinforced concrete (RC) tunnel rings in fire. The modelling of fire exposed RC tunnel rings is carried out using a sequentially coupled thermo-mechanical analysis. To reduce the computational effort, a plane model is chosen for the tunnel lining to demonstrate the non-linear behaviour of tunnel rings from the fire load.

2.1 General procedure

Fig. 1 illustrates the analysis and design procedure for a shield tunnel structure subjected to fire. At different stages of the analysis, various input parameters need to be provided. Firstly the tunnel fire scenarios and equations of transient heat conduction should be specified in the heat transfer analysis. A temperature–time curve representing the fire at the heating surface needs to be defined, noting that the commonly prescribed structural design fires are defined by gas phase time-temperature curves, e.g. ISO834, HC, RABT-ZTV, RWS standard curves (Maluk et al., 2019). The tunnel cross section is divided into different regions to account for the variance in elevated temperatures across the height (Hua et al., 2022). To be more specific, during a tunnel fire, the heat transfer of the vault surface is always identified as the hottest region, and that of the shoulder's regions is determined through a weaker heat convection and radiation mode. The bottom region, which isolated by substructures, is defined as insulation. Following the transient heat transfer analysis, the temperature distribution within the segments at each time step is obtained. As the thermal analysis is independent of the stress states, the model cannot predict directly the effect of concrete spalling. Following the consideration that the first indication of spalling from experimental findings (Hua et al., 2022), the deactivation of layers at the inner side of the tunnel lining was assumed to be mainly caused by spalling during the in-fire rapid thermal shock (Savov et al., 2005; Hua et al., 2021).

In the mechanical analysis of the tunnel structure, the non-linear transient thermal-mechanical coupled numerical analysis requires considerable effort. Apart from the pre-calculated temperature input, the time-dependent loads and ground constraints need to be defined in the model in accordance with the tunnel's surrounding geological conditions. Since the thermo-mechanical analysis is "sequentially-coupled" and the coupling between the two simulations is internally managed by the FEM codes, the finite element discretization is kept constant, while the element type changes from thermal to structural elements for the thermal and mechanical analysis, respectively. In other words, the time-dependent temperature of each element is obtained from the thermal analysis, which then serves as an input for the subsequent mechanical analysis. The stress field in concrete is derived from the corresponding mechanical strain, suitably corrected by including the contribution of the free thermal strain, which is considered stress independent and isotropic.

2.2 Element types

Following the general procedure, a thermo-mechanical analysis is conducted using finite element software ABAQUS (ABAQUS, 2014) to determine the transient nodal temperatures. In the heat transfer analysis, all materials are continuous, isotropic and without any internal heat source. The effect of moisture evaporation in the concrete lining structure on the heat conduction process is not considered. A two-node heat transfer element (DC1D2) is used for steel bars and bolts, and the plane heat transfer elements (DC2D4) are used for concrete. Compared with solid elements, the two-dimensional elements are more computationally efficient for both the thermal and structural models for the prediction of the temperature distribution, and similar modelling strategies have been adopted in the past (Chang et al., 2016; Choi et al., 2013). A tie constraint is used to apply temperatures from concrete to reinforcing steel bars and bolts at the same location. The external surface areas of DC2D4 elements, which are exposed to fire from one side, are used to simulate the surface effect of convection and radiation that occur from fire (ambient air) to the segments. The model of shield tunnel structure is mainly composed of concrete segments, bolts and steel bars. In the analysis model, a two-node truss element (T2D2) is used for steel bars, a beam element (B21) is used for bolts and a plane strain element (CPE4R) is used for concrete. As the model involves a large number of parts and that complex interaction exists between different parts, the phenomenon of stress concentration could easily occur in the simulation analysis.

For the segmental joint, the contact between segments is set as face-to-face contact, with the normal direction set as hard contact, and the tangential direction set with friction "rough" to limit tangential dislocation on both sides of the joint. The constraint relation between reinforcement and segmental concrete is set as embedded contact. The constraint between bolt and segment concrete is complicated, thus it is set as a partially embedded constraint, and the contact surface and related parameters are adjusted to the expandable state. Only the main reinforcement in the segment is considered. All the bolts are modelled with a nonlinear element connector. The elastic sealing pad and water strip at the joint are ignored.

2.3 Material models

For common shield tunnel structures, the main constituent materials are concrete and steel, whose thermal and mechanical properties vary with elevated temperatures. These input parameters are very crucial to the evaluation of the vulnerability of a tunnel to fire hazard considering all critical aspects that could influence a tunnel structure's performance in fire. Presented thermal and mechanical properties at different target temperatures are incorporated into equations or tables in Eurocode 2 clearly to obtain the specific value (Le et al., 2021). Following the temperature-dependent thermal properties defined in Eurocode 2 (CEN, 2004), the specific heat, thermal conductivity and coefficient of thermal expansion of reinforcing steel and concrete are listed in **Table A1** in **Appendix A**.

For the stress-strain relationship of concrete and reinforcing steel, the instantaneous stress-related strain and thermal strain are evaluated according to EC2 (CEN, 2004). Considering the nonlinearity and different failure mechanisms under compression and tension, a damaged plasticity constitutive model is employed to model the complex behaviour of concrete. The envelop stress-strain relation for concrete is represented by a bilinear relationship, consisting of an elastic part up to the peak stress and then a stable part until the ultimate strength. The ultimate strength at elevated temperatures is assumed to vary as per EC2 (CEN, 2004). The variation of mechanical and thermal properties with respect to temperature is different in the cooling phase as compared to the heating phase and it depends on the maximum temperature reached during the heating phase. During the cooling phase, a linear interpolation between the elevated and residual material properties after cooling down is adopted. Following the specifications in Eurocode 2 (CEN, 2004), the temperature dependant mechanical properties adopted in this study are listed in **Table A1** in **Appendix A**..

2.4 Boundary conditions

Thermal analysis is performed in order to obtain the transient temperature field within the tunnel. This analysis takes into account all the three mechanisms governing the heat transfer, namely conduction, convection and radiation. The heat transfer from a fire source to the surface of a structural member is through convection and radiation. The heat flux to the surface of a structural member through radiation and convection is expressed as boundary conditions in the thermal analysis. The heat transfer within a structural member is through conduction, which is expressed as a Fourier heat transfer equation. The general differential equation for the heat transfer in a structural member can be expressed as:

$$\frac{\lambda}{\rho c}\nabla^2 T = \frac{\partial T}{\partial t} - \frac{Q}{\rho c} \qquad (1)$$

where ρc is the heat capacity of the section, λ is the thermal conductivity tensor, t is time, T is temperature, ∇ is spatial gradient operator, and Q is internal heat generation rate per unit volume. The heat flux on the fire-exposed boundary due to convection and radiation can be expressed by the following equation:

$$Q = \left(h_{con} + h_{rad}\right)\left(T - T_f\right) \qquad (2)$$

where h_{con} and h_{rad} are convective and radiative heat transfer coefficients, T_f is fire temperature. Heat transfer problems involving conduction, forced convection, and boundary radiation can be analysed by a numerical calculation procedure.

For most metro shield tunnels, the inner diameter of the tunnel section is usually below 6 m and the lining around the tunnel, except the thick track base layer at the bottom, is considered to be directly exposed to the thermal range of fire. Therefore, when considering a tunnel fire, the thermal boundary conditions can be directly applied to the lining surface, whereas the tunnel lining structure under the bottom track base layer may be considered as not being influenced by the elevated temperatures. Since the heat convection and radiation of a tunnel fire source to the surrounding wall surface are not uniform, dividing the tunnel inner wall into multiple temperature zones can improve the accuracy of calculation of the lining thermal boundary (Guo et al, 2019). Based on the above considerations and the actual heating conditions of subway tunnels, the lining thermal boundary is divided into three sections as shown in **Fig. 2** (a). More specifically, Section I is strongly and directly affected by the fire source, and is the heat conduction affected area; Section II is mainly affected by convective heat of the fire source, and is the affected zone of thermal convection. Section III is considered as an adiabatic zone due to the insulation of the trackbed base. All the above thermal boundary distribution T in a symmetric half-circle space can be expressed by the following equation:

$$\begin{cases} T(\theta) = \overline{T}(t'), & \theta \in [0, 45°) \\ \boldsymbol{q} \bullet \boldsymbol{n} = h \left| T(\theta) - \overline{T}(t') \right|, & \theta \in [45°, 150°) \\ \left. \dfrac{\partial T(\theta)}{\partial n} \right|_{\theta} = 0, & \theta \in [150°, 180°] \end{cases} \tag{3}$$

where θ represents the range of the central angle of the temperature boundary, $\overline{T}(t')$ is the temperature rise curve function of the fire source, $\boldsymbol{q}$ is the heat flow vector of the tunnel boundary in the vector $\boldsymbol{n}$ direction, and h (W/m^2·K) is the convective heat transfer coefficient. According to the previous experimental and calculation results (Yao et al., 2021), the convective heat transfer coefficient is taken to be 25 $W/m^2 \cdot K$ on a fire exposed surface. The emissivity for the radiative heat transfer at the exposed surfaces of the tunnel lining segments is taken as 0.8.

The mechanical load configuration for the shield tunnel is presented in **Fig. 2**(b). Since the focus of this work is the evaluation of tunnel behaviour under fire conditions, the simulation of tunnel installation phases is herein simplified, such that only the final equilibrium condition between the support system and the surrounding ground is considered, which is typical of a service-state condition. The structural capacity of the tunnel lining segment at the ultimate limit state (ULS) for bending and axial actions is typically represented by a moment-axial force interaction curve (M-N curve). The soil-structure interaction is modelled with spring elements that transfer only the compression-action and have a zero lift-off tension capacity. The radial spring compression stiffness can be obtained from a geotechnical investigation report, or generally calculated using the following equation:

$$K_R = \frac{E}{R} \cdot \frac{1-\nu}{(1+\nu)(1-2\nu)} \tag{4}$$

where K_R is the radial spring stiffness, E is the Young's Modulus of the ground, R is the tunnel radius and ν is the Poisson's ratio of the ground.

In the structural analysis of a shield tunnel, appropriate failure criteria should be applied for the applicable failure limit states. For evaluating the capacity of the tunnel at an ambient condition or under fire exposure, the strength limit state generally governs the failure but a deflection limit state is often a reliable failure indicator from a performance perspective. Accordingly, the failure of the tunnel structure is said to occur (NSC, 2021) when the maximum convergence deformation of shield tunnel exceeds 0.2% of the central diameter, or the maximum opening of the joints exceeds 2 mm. It is important to note here that the aforementioned deflection limit states have been developed for common shield tunnels, with an inner diameter below 10 m, and may not be strictly applicable under a fire scenario. In this respect, the timescale leading to failure from the analysis with the above deflection-based limits would generally be on the conservative side.

3. Model verification

After the model is established, an appropriate verification against suitable experimental results is required. Experimental data on fire growth characteristics and temperature-dependent structural responses need to be collected to validate the numerical model. As shown in **Fig. 1**, the shield segments and the joints are key elements in the whole tunnel rings; therefore, a comparison of the temperature profile in the segments between the numerical analysis and actual experiment can be instructive on the adequacy of the numerical model. The accuracy of numerical analysis in terms of the mechanical behaviour may be evaluated by comparing the deformations of segments and joints with those from the experiments.

3.1 Overview of relevant experimental tests

RC segments and RC segmental joints tested by the authors' research group (Yan et al. 2015; Yan et al. 2016) are selected to validate the numerical model presented in Section 2. The test system has been developed for testing shield tunnel segments and joints under both applied mechanical loads and elevated temperatures. In the test system, a furnace powered by two combustors of industrial grade can be controlled by a programmable controller to achieve a desired heating up history. The test system can provide a wide range of combinations of mechanical loading and fire scenarios, including high rate heating (250 °C/min) and high peak temperature (1200°C) in conjunction with diverse mechanical load patterns.

In the aforementioned tests, the furnace temperature was all monitored and controlled to follow the standard Eurocode HC curve (CEN, 2002). The test specimens represented metro shield tunnels at a reduced scale of about 1:3 with respect to the full-size lining units. Thus, the test specimens were 120 mm in thickness and 300 mm in width, and the average radius of the assembled ring was 990 mm. The size of the specimens allowed the composition of the materials in the actual construction to be maintained in the test specimens, thus avoiding any material scaling effect. The materials used in the preparation of the test specimens, including concrete, the main reinforcement and bolts, are the same as the actual shield tunnel lining structure. These tests are selected for validation because comprehensive results have been reported, and the representative cases can facilitate finite element simulations and detailed comparisons. RC segments and segmental joints tested under fire exposure are analysed by applying the above numerical procedure to validate the proposed approach.

3.2 Verification of temperature field analysis

A comparison of the temperature results between the numerical calculation and the test data is shown in **Fig. 3**. It can be observed that towards the later part of the first 60 min the numerical and experimental results show good agreement. However there is some noticeable difference between the test temperature and the numerical results at 10mm and 30mm during the rising process. This is because in the physical structure the lining concrete will lose free water and calcium silicate hydrate (C-S-H) will lose bound water when heated (Zhao et al., 2014), thus forming a temperature platform above and below the boiling point of water. The temperature rises rapidly as the water in the area evaporates. On the other hand, in the numerical analysis a homogenous model is employed with the thermal properties as given in EC2 (CEN, 2004). Due to the complex heat transfer process in actual concrete, there is no simple equivalence in the heat transfer parameters in using a homogeneous model. Consequently, the temperature development process from the numerical model can be anticipated to show variation from the actual situation in concrete specimens during a fire test. Nevertheless, the temperature development will become smooth and steady afterwards as the maximum temperature of HC curve is 1100 °C and it has almost been reached at the closest point (10mm) exposed to fire. In addition, the simulation time of the numerical calculation conditions is set as long as two hours or more (Choi et al., 2013), so any discrepancy in the earlier process of temperature development will not affect significantly the structural response results and the comparative discussion.

3.3 Verification of structural analysis

Figs. 4 and **5** show the comparisons between the numerical and experimental results in terms of the vertical load vs. midspan displacement and vertical load vs. joint inner opening relationships. Very good agreement can be observed, indicating that the numerical model simulates well the mechanical behaviour of segments at elevated temperatures.

4. Parametric study and discussions

In this section, a typical shield tunnel case is analysed using the modelling framework presented in Section 2. The influences of the key parameters on the performance of shield tunnel rings are examined through the parametric analysis and the results are discussed.

4.1 Model configuration

The shield tunnel structure of Shanghai Metro Line No. 14 is chosen in this case study. The concrete type is C55, the main reinforcement grade is HRB400 and the bolt grade is 5.8. The external diameter of the tunnel lining is 6.20 m, and the inner diameter is 5.50 m. The ring width and thickness are 1.20 m and 0.35 m, respectively. Each ring consisted of one key segment (F), two adjacent segments (L_1 and L_2), two standard segments (B_1 and B_2), and one counter key segment (D), as shown in **Fig. 6**.

The stratum parameters are obtained from the geological exploration data of Shanghai rail transit, as summarised in **Table 1**. The groundwater level is 0.5m below the filled soil layer. According to the general design provisions of this area, the buried depth for shallow, medium and deep buried tunnels is 6.5m, 15.6m, and 23.5m, respectively. For spalling estimation, the average depth can be assumed to be 40 mm (Monckton, 2018). In general correction practices, isosceles triangle loads are used to simulate the formation reactions. Such calculation is considered reasonable at room temperature, but under the action of high temperature in a fire scenario, the tunnel structure will produce different degrees of compression to the surrounding soil, especially for the vault position where the temperature increases rapidly. Therefore, soil springs need to be placed around the tunnel in a high temperature model, so as to represent the constraints of the stratum on the structure. According to the exploration data of relevant sections and the empirical data of shield tunnel segment design, 20kN/m^3 is taken for the sandy silt and 5kN/m^3 for the soft clay.

HC and RABT heating curves represent two typical fire boundary conditions with a high heating rate and a cooling stage respectively. The standard Eurocode HC curve and RABT curve adopted herein to simulate the heating phase are expressed in Eqs. (5) and (6), respectively:

$$T(t)=20+1080(1\text{-}0.325\mathrm{e}^{-0.167t}\text{-}0.675e^{-2.5t}) \tag{5}$$

$$T(t)=\begin{cases} 20+236t & 0\le t\le 5 \\ 1200 & 5\le t\le 130 \\ 1200-10.727(t-130) & 130\le t\le 240 \end{cases} \tag{6}$$

where t is time (in minutes) and $T(t)$ is the gas temperature inside the furnace (in °C).

The applied loads on tunnels with different buried depths and surrounding strata are different, so the safety under fire in each depth case should be evaluated separately. The numerical simulation cases are listed in **Table 2**.

4.1 Influence of spalling

Structural members in a tunnel under severe fire exposure may experience significant deformations and structural damage caused by temperature-induced forces, resulting in phenomena like spalling in concrete and rupturing of connections. In moderate- to low-intensity fire scenarios, deformations or damage in structural members may not be significant, but localized damage such as spalling in concrete linings can still occur. The application of inner surface insulation is assumed herein due to the heat insulation practice in actual tunnels.

Fig. 7 shows the temperature of F segment inner reinforcement vs time under HC and RABT fire curves, respectively. It can be seen that there is a marked increase of the reinforcement temperature if spalling occurs. After the explosive spalling, the inner reinforcement exhibits a rapid rise in temperature to more than 1000℃ and consequently loses its bearing capacity. If the inner reinforcement completely loses its bearing capacity, the lining concrete will share more loading under fire, leading to further damage to the structure and even failure.

The joints of the tunnel structure are also key elements in the tunnel structure. **Fig. 8** (a) and (b) show the temperature variation of F-L_1 bolt and L_1-D_1 bolt with time under HC curve and RABT curve, respectively. It can be seen from **Fig. 8** (a) that under the HC curve, the bolt temperature increases at a significantly higher rate after the spalling, and the maximum temperature reaches nearly 480℃, nearly twice as high as that before the spalling. What stands out in **Fig. 8** (b) is that although there is a cooling stage in the RABT curve, the temperature of the joint is still about 150℃ at 4h, which is higher than that of the joint without spalling. When the temperature increases sharply, the yield stress of the joint bolt decreases and the temperature strain increases, and this makes it quicker for the joint to reach the critical state.

Fig. 9 (a) and (b) show the maximum displacement of the vault of the tunnel under the HC and RABT fire curve, respectively. It can be seen that the maximum displacement after spalling peaks at 32 mm. It is worth noting that there is a 4 mm increment than that without spalling, this results in the convergence deformation of tunnel approaching the limit state. As shown in **Fig. 9** (b), under the RABT curve and after spalling, the tunnel structure even exceeds the limit deformation and reaches total failure after 67min. A possible reason is that the opening process of F-L_1 and F-L_2 joints gradually shifts from inside to outside during the continuous fire in the deep tunnel. The displacement change of the vault is influenced by the deformation of the joint bolts. The deformation of the joint bolts increases as the temperature rises after spalling, and this in turn leads to further deformation of the vault.

4.2 Influence of buried depth

Fig. 10 shows the vertical displacements of shallow, medium and deep tunnel structures. The initial displacements are 3 mm, 6 mm and 12 mm for the three depths, respectively. Under the action of the HC curve with a continuous temperature rising, the vertical displacements of the structural vault all decrease first and then increases. Because the elevation of temperatures has a certain delay in causing damage in the structural materials, it can be deduced that the thermal expansion response is the main factor affecting the structural deformation in the early stage of the fire. However, since the interior opening of the F-L_1 and F-L_2 joints is recovered from thermal expansion first, the displacement at the top of the tunnel structure does not develop outward. After the interior opening of the joints is recovered, the vault of the tunnel structure begins to expand outward. For this reason, it can be seen from **Fig. 10** that the vertical displacement of the deep buried tunnel with the largest interior opening of F-L_1 and F-L_2 joint dramatically decreases, and the maximum displacement also reaches about 31mm, which exceeds the limit state of the tunnel structure and is close to destructive damage. In addition, the descending phase of the vertical displacement of the deep buried tunnel is as long as 120 min, and the effect of thermal expansion of the lining inner layer of the tunnel structure is nearly saturated. In comparison, the rising rate of the ascending branch of the vault displacement in the deep buried tunnel is far less than that of shallow and medium buried tunnels.

When the tunnel is under the RABT curve (**Fig. 10**(b)), the vertical displacement of the vault of the tunnel at each buried depth is basically maintained after a short recovery in the cooling stage. The vertical displacement of the vault in the case of deep-buried tunnel cannot be recovered, and this could pose a serious threat to the structure safety in the cooling stage.

There is also a close correlation between the amount of opening in the key joints of the tunnel structure and the buried depth. The change of the amount of opening in L_1-B_1 joints under different buried depths is shown in **Fig. 11**. Under ambient temperature, the joint opening of the tunnel structure with a larger buried depth tends to be larger, but compared with the joint opening in fire, the initial joint opening is relatively small and hence the differences may be ignored. As shown in **Fig. 11** (a), during the 90 min period after the initiation of fire, the opening of L_1-B_1 joints of all buried tunnels increases rapidly, and the subsequent increase rate slows down. The increase rate of the shallow-buried tunnel is less than that of medium- and deep-buried tunnels in the stage of the rapid expansion of the joint opening, and the final opening is only about 60% of that of medium- and deep-buried tunnels. It can be seen that although the opening of L_1-B_1 joint is different in the initial state due to the influence of load combinations caused by the buried depth of the tunnel, the main factor influencing the variation of joint opening is still the stratum spring. Due to the weakness of the surrounding strata, the constraint on the expansion deformation of the tunnel structure under fire is flexible, and this makes the deformation of the joints larger. Interestingly, as can be seen from **Fig. 11** (b), under the action of RABT curve with a cooling stage, the opening of L_1-B_1 joint recovers significantly when cooling sustains for 40 min, and the recovery speed of the joint opening of the medium- and deep-buried tunnels is faster than that of the shallow-buried tunnel. The opening of tunnels with different depths eventually tends to be the same in the last period of cooling. The above results reveal that the influence of the buried depth on the deformation of key joints mainly exists in the heating stage of fire, and it is not significant in the cooling stage.

4.3 Influence of cooling-off phase

Fig. 12 shows the temperature distributions in the tunnel structure. It can be seen that the elevated temperatures induced by fire gradually penetrated the lining, and the heat insulation surface under the track bed gradually heated up. However, there are no apparent differences in the temperature at the interface between the direct heat transfer section and the heat convection-dominated section. For the tunnel under the RABT curve, the development of the temperature field through the thickness of the lining begins to decline during the cooling phase, but part of the tunnel still reaches a high temperature. At the time of 4 h, i.e., cooling after 110 min, the area with a remaining temperature of 200~400 ℃ is still extensive. In other words, although the fire risk has disappeared at this point of time, the hidden danger of the tunnel structure still exists. As can be seen in detail from **Fig. 13**, for the sections of vault and sidewall, only the points with a depth of less than 10cm into the thickness experience an apparent cooling stage. The temperature in the lining with a depth between 20 cm and 35 cm almost maintains a linear increase in the whole process and there is no slow-down in the heating trend during the cooling process. After cooling for 110min, the temperature at the depth of 20 cm rises to more than 100℃, and the temperature at 200-400 ℃ is distributed in the 5-15cm depth of the lining thickness. When the lining structure reaches such a level of temperature, the internal force of the structure induced by thermal expansion and the degradation of the mechanical properties of the material are not negligible factors for the mechanical behaviour of the structure. Therefore, for the tunnel structure under the RABT curve, it is necessary to consider the fire-induced mechanical response not only in the heating process but also in the cooling process.

Fig.14 shows the deformation contours of the shallow-buried tunnel structure. It can be seen that before the cooling stage, the deformation of the structure under the RABT fire curve is similar to that under the HC curve. After the cooling stage, the overall deformation of the structure tends to be steady without further deformation, but there is no significant recovery. From the detailed joint opening deformation history shown in **Fig.15**, the opening of joint F-L_1 and joint B_1-D does not change significantly until a period after the start of the fire, while the opening of L_1-B_1 joint increases rapidly after the start of the fire and finally reaches 9mm. Although the deformation at the sealing pad of each joint is reduced in the cooling stage, the amount of reduction is quite small. The above results indicate that, following a fire, the residual capacity of structural members must be comprehensively evaluated in order to assess the damage and safety of the tunnel structure. Setting up specifically designed sprinklers or water curtain systems will effectively control the initial fire development and shorten the cooling-off phase. Integrating structural fire design principles into the structural design of tunnel components can significantly enhance the inherent fire resistance of tunnel structures.

5. Conclusions and future work

In this paper, a thermo-mechanical framework is presented for a holistic analysis of the structural response of assembled shield tunnel rings in fire. The analysis framework incorporates the tunnel lining segments and longitudinal joints to improve the predictions for the temperatures, stresses and deformations of the tunnel structure. The approach is validated by comparison of the predicted responses with previous experimental results. A parametric study is performed to demonstrate the influences of key parameters on the load and fire effects on shield tunnel structure. The following conclusions can be drawn:

（1） The damage and failure of a shield tunnel ring structure under high temperature are mainly due to a combined action of internal thermal expansion force and thermal stress.

The most critical areas of the ring structure in fire are the vault and the key joints L1-B1 and L2-B2 of the shoulder’s regions. In the early stage of fire development, the arch region of the ring sustains a substantial deformation development and incurs large deflection. With the continuation of the fire, the large lateral opening angle in the key joints tends to result in a progressive failure, while water and soil could pour through the joints to induce sudden local damage.

（2） The spalling of concrete results in a loss of important “insulation” layer for the tunnel lining structure. As a result, the inner steel bar of the lining tends to completely lose its bearing capacity under fire. The strength of the bolts at the joints also decreases with the increasing temperature strain. The lining concrete tends to be subjected to increased loading under the fire, and this puts further demand on the structure, leading to accelerated failure.

（3） From the parametric study, it is found that the influence of different buried depths on tunnel structures under fire mainly come from two aspects, namely different load combinations and different ground spring resistance coefficients. The constraint of strata on the structure under high fire temperature not only restrains the deformation of the key parts of the structure, but also offsets the adverse effect of load on the structure through elastic resistance. This mechanism is deemed to be a key factor affecting the safety and durability of tunnel structure under fire.

（4） Comparison analyses between two heating curves, i.e. the HC curve and the RABT curve, reveal that under elevated temperatures, the stress state in the F segment, the L segments, and the B segments gradually changes into a full section compression. The areas that mainly bear compressive stress expand and move outward, forming an arched high-stress area. On the other hand, the stress state of the inner side of the concrete lining gradually changes from compression to tension in the cooling stage, but most areas are still in a compression state. Furthermore, the stress recovery process caused by cooling is relatively slow, therefore it will still be necessary to exercise caution, and careful evaluation should be carried out on the residual state of the tunnel structure after the fire.

（5） The analysis results suggest that the stiffness of the assembled tunnel ring plays a dominant role in maintaining the structural fire safety. A possible strategy to enhance the stiffness can involve retrofitting the construction of longitudinal joints to reduce the deformation under elevated temperatures.

For future research in evaluating the fire performance of the shield tunnel structure it will be useful to look into the impact of circumferential joints and the settlement of tunnels. Hybrid fire testing incorporating nonlinear substructure experiments and numerical analysis are also being planned as part of our future work.

Acknowledgements

The authors wish to acknowledge the sponsorship from Shanghai Sailing Program (20YF1451400), and the Research Fund of State Key Laboratory for Disaster Reduction in Civil Engineering (SLDRCE19-A-14).

References

ABAQUS Standard User's Manual. Version 6.14, vol. I–III. Pawtucket (America): Hibbitt, Karlsson & Sorensen, Inc.; 2014.

Alhawat H, Hamid R, Baharom S, Azmi M R, Kaish A B M A, 2021. Thermal behaviour of unloaded concrete tunnel lining through an innovative large-scale tunnel fire experimental testing setup. Construction and Building Materials. 283: 122718.

Beard, A., Carvel, R., 2011. Handbook of Tunnel Fire Safety, 2nd edition, ICE Publishing, London.

Bergmeister, K., Brunello, P., Pachera, M., Pesavento, F., Schrefler, B.A., 2020. Simulation of fire and structural response in the Brenner Base Tunnel by means of a combined approach: A case study. Engineering Structures 211, 110319.

Carvel, R., 2019. A review of tunnel fire research from Edinburgh. Fire Safety Journal. 105, 300-306.

Casse, C., Caroly, S., 2019. Analysis of critical incidents in tunnels to improve learning from experience. Safety Science. 116, 222–230.

CEN, 2002. Eurocode 1: Actions on structures, EN 1991-1-2. London: British Standards Institution..

CEN, 2004. Eurocode 2. Design of concrete structures, 1992-1-2. London: British Standards Institution.

Chang, S., Choi, S., Lee, J., 2016. Determination of the combined heat transfer coefficient to simulate the fire-induced damage of a concrete tunnel lining under a severe fire condition. Tunnelling and Underground Space Technology 54, 1-12.

Chen, F., Chien, S.W., Lee, Y.P., Lin, C.F., Sie, H.R., 2013. The integrated strategies for fire safety of long road tunnels in Taiwan. Procedia Engineering 62, 36–45.

Choi, S., Lee, J., Chang, S., 2013. A holistic numerical approach to simulating the thermal and mechanical behaviour of a tunnel lining subject to fire. Tunnelling and Underground Space Technology 35, 122-134.

Colombo, M., Martinelli, P., di Prisco, M., 2015. A design approach for tunnels exposed to blast and fire. Structural Concrete 16, 262-272.

Du, S., Zhang, Y., Sun, Q., Gong, W., Geng, J., Zhang, K., 2018. Experimental study on color change and compression strength of concrete tunnel lining in a fire. Tunnelling and Underground Space Technology 71, 106-114.

Guo, Q., Root, K.J., Carlton, A., Quiel, S.E., Naito, C.J., 2019. Framework for rapid prediction of fire-induced heat flux on concrete tunnel liners with curved ceilings. Fire Safety Journal 109, 102866.

Hua, N., Tessari, A., Elhami Khorasani, N., 2021. Characterizing damage to a concrete liner during a tunnel fire. Tunnelling and Underground Space Technology. 109: 103761.

Hua, N., Tessari, A., Elhami Khorasani, N., 2022. The effect of geologic conditions on the fire behavior of tunnels considering soil-structure interaction. Tunnelling and Underground Space Technology 122, 104380.

Kodur, V. R., Naser, M. Z., 2020. Structural Fire Engineering. McGraw Hill Education.

Le, Q.X., Torero, J.L., Dao, V.T.N., 2021. Stress–strain–temperature relationship for concrete. Fire Safety Journal 120, 103126.

Lilliu G, Meda A. Nonlinear Phased Analysis of Reinforced Concrete Tunnels Under Fire Exposure. Journal of Structural Fire Engineering. 2013, 4(3): 131-142.

Maluk, C., Bisby, L., Krajcovic, M., Torero, J.L., 2019. A Heat-Transfer Rate Inducing System (H-TRIS) Test Method. Fire Safety Journal 105, 307-319.

National Standard of China, GB/T 51438-2021, 2021. Standard for design of shield tunnel engineering. Beijing: China Architecture & Building Press. (in Chinese)

Monckton, H., 2018. Practical design, testing & verification guidelines for pre-cast segmental tunnel linings subjected to fire loading. Tunnelling and Underground Space Technology 77, 237-248.

Ouyang, Z., Guo, Q., Quiel, S.E., Naito, C.J., 2021. Vulnerability of Drop Ceilings in Roadway Tunnels to Fire-Induced Damage. Transportation Research Record: Journal of the Transportation Research Board, 862849094.

Qiao, R., Shao, Z., Liu, F., Wei, W., 2019. Damage evolution and safety assessment of tunnel lining subjected to long-duration fire. Tunnelling and Underground Space Technology 83, 354-363.

Ren, R., Zhou, H., Hu, Z., He, S.Y., Wang X.L., 2019. Statistical analysis of fire accidents in Chinese highway tunnels 2000–2016. Tunnelling and Underground Space Technology., 83 452-460.

Ring, T., Zeiml, M., Lackner, R., 2014. Underground concrete frame structures subjected to fire loading: Part I – Large-scale fire tests. Engineering Structures 58, 175-187.

Savov, K., Lackner, R., Mang, H. A., 2005. Stability Assessment of Shallow Tunnels Subjected to Fire Load. Fire Safety Journal, 40: 745-763.

Shen, Y, Zhu, H, Yan, Z, Zhou, L, Lu, Y., 2021. Semi-analytical thermo-mechanical model for the shield tunnel segmental joint subjected to elevated temperatures[J]. Tunnelling and Underground Space Technology. 118: 104170.

Tomar, M.S., Khurana, S., 2019. Impact of passive fire protection on heat release rates in road tunnel fire: A review. Tunnelling and Underground Space Technology 85, 149-159.

Yan, Z, Zhu, H, Ju, J. W., 2013. Behavior of reinforced concrete and steel fiber reinforced concrete shield TBM tunnel linings exposed to high temperatures. Construction and Building Materials, 38, 610-618.

Yan, Z., Shen, Y., Zhu, H., Li, X., Lu, Y., 2015. Experimental investigation of reinforced concrete and hybrid fibre reinforced concrete shield tunnel segments subjected to elevated temperature. Fire Safety Journal, 71, 86-99.

Yan, Z., Shen, Y., Zhu, H., Lu, Y., 2016. Experimental study of tunnel segmental joints subjected to elevated temperature. Tunnelling and underground space technology, 53, 46-60.

Yan, Z., Zhang, Y., Shen, Y., Zhu, H., Lu, Y, 2020. A multilayer thermo-elastic damage model for the bending deflection of the tunnel lining segment exposed to high temperatures. Tunneling and Underground Space Technology, 95, 103142.

Yan, Z., Zhu, H., Ju, J. W., Ding, W., 2012. Full-scale fire tests of RC metro shield TBM tunnel linings. Construction and Building Materials, 36, 484-494.

Yao, Y., He, K., Peng, M., Shi, L., Cheng, X., 2021. The maximum gas temperature rises beneath the ceiling in a longitudinal ventilated tunnel fire. Tunnelling and Underground Space Technology 108, 103672.

Zhang, T., Zhang Y., Zhu, H., Yan, Z., 2021a. Experimental investigation and multi-level modeling of the effective thermal conductivity of hybrid micro-fiber reinforced cementitious composites at elevated temperatures. Composite Structures, 256, 112988.

Zhang, T., Zhang, Y., Zhu, H., Yan, Z., 2021b. Characterizing the thermal properties of hybrid polypropylene-steel fiber reinforced concrete under heat exposure: Insights into fiber geometry and orientation distribution. Composite Structures, 275, 114457.

Zhang, T., Zhu, H., Zhou, L., Yan, Z., 2021c. Multi-level micromechanical analysis of elastic properties of ultra-high performance concrete at high temperatures : Effects of imperfect interface and inclusion size. Composite Structures, 262, 113548.

Zhang, X., Wu, X., Park, Y., Zhang, T., Huang, X., Xiao, F., Usmani, A., 2021d. Perspectives of big experimental database and artificial intelligence in tunnel fire research. Tunnelling and Underground Space Technology 108, 103691.

Zhang, Y., Zhu, H., Guo, Q., Carvel, R., & Yan, Z., 2021e. The effect of technical installations on evacuation performance in urban road tunnel fires. Tunnelling and Underground Space Technology, 107, 103608.

Zhao, J., Zheng, J.J., Peng, G.F., 2014. A numerical method for predicting young's modulus of heated cement paste. Construction and Building Materials, 54 (54), 197–201.

Table 1 Soil parameters of a section of Shanghai Metro Tunnel

Stratum	Thickness (m)	Unit weight (kN/m^3)	Cohesion (kPa)	Internal friction angle(°)	Coefficient of ground spring (kN/m^3)
Fill ①$_1$	1.9	18	-	-	-
Sandy silt ②$_{3-1}$	1.9	18.6	5	30.5	20
Sandy silt ②$_{3-2}$	4.2	18.3	5	30.5	20
Sandy silt ②$_{3-3}$	4.7	18.3	4	31.5	20
Silty clay ④	5.3	17	14	12.5	2
Clay ⑤$_{1-1}$	3.8	17.6	15	13.5	2
Clay ⑤$_{1-2}$	8	17.9	15	13.5	2

Table 2 List of numerical simulation cases

No.	Heating curves	Duration	Burial depth	Spalling
A1	HC	4h	Shallow	⊗
A2	HC	4h	Medium	⊗
A3	HC	4h	Deep	⊗
AS1	HC	4h	Shallow	☑
AS2	HC	4h	Medium	☑
AS3	HC	4h	Deep	☑
B1	RABT	4h	Shallow	⊗
B2	RABT	4h	Medium	⊗
B3	RABT	4h	Deep	⊗
BS1	RABT	4h	Shallow	☑
BS2	RABT	4h	Medium	☑
BS3	RABT	4h	Deep	☑

Note: ☑:Spalling; ⊗:No spalling.

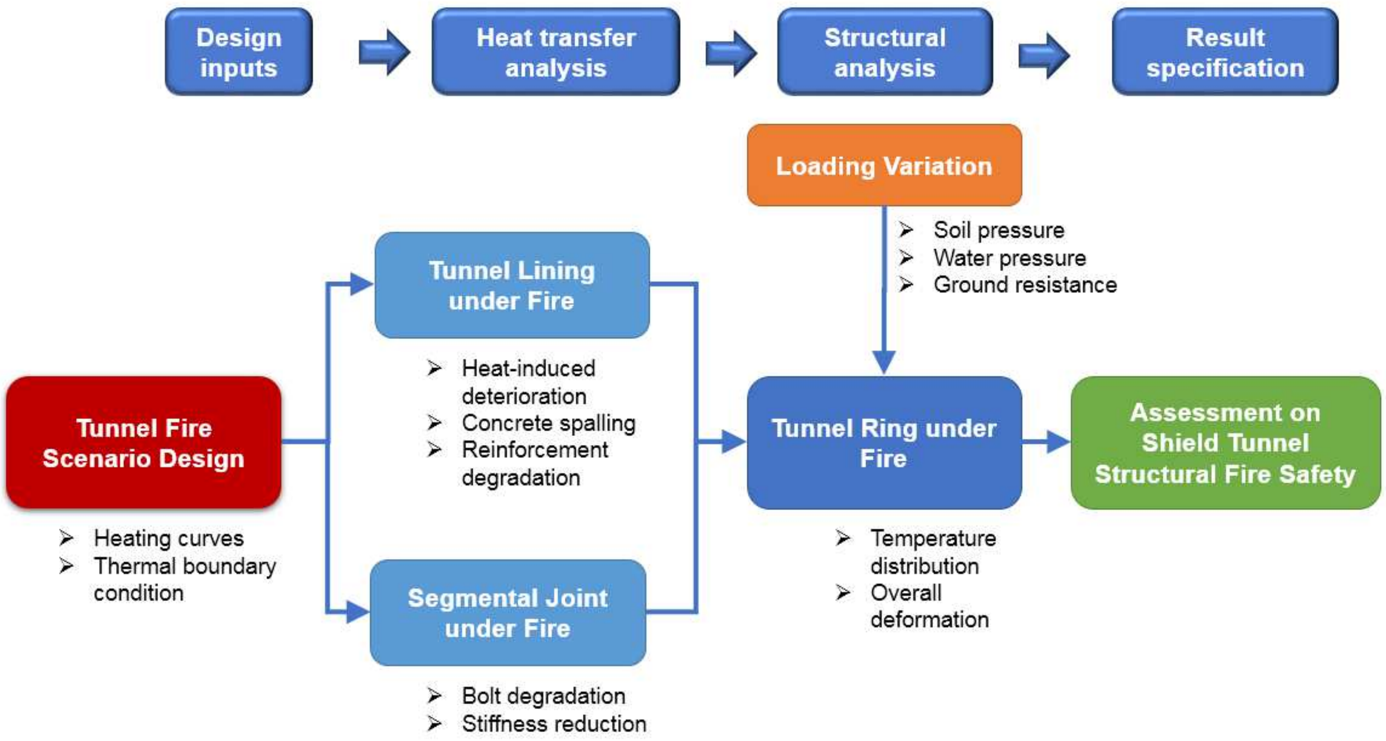

Fig. 1 Analysis and design procedure of shield tunnel structure in fire.

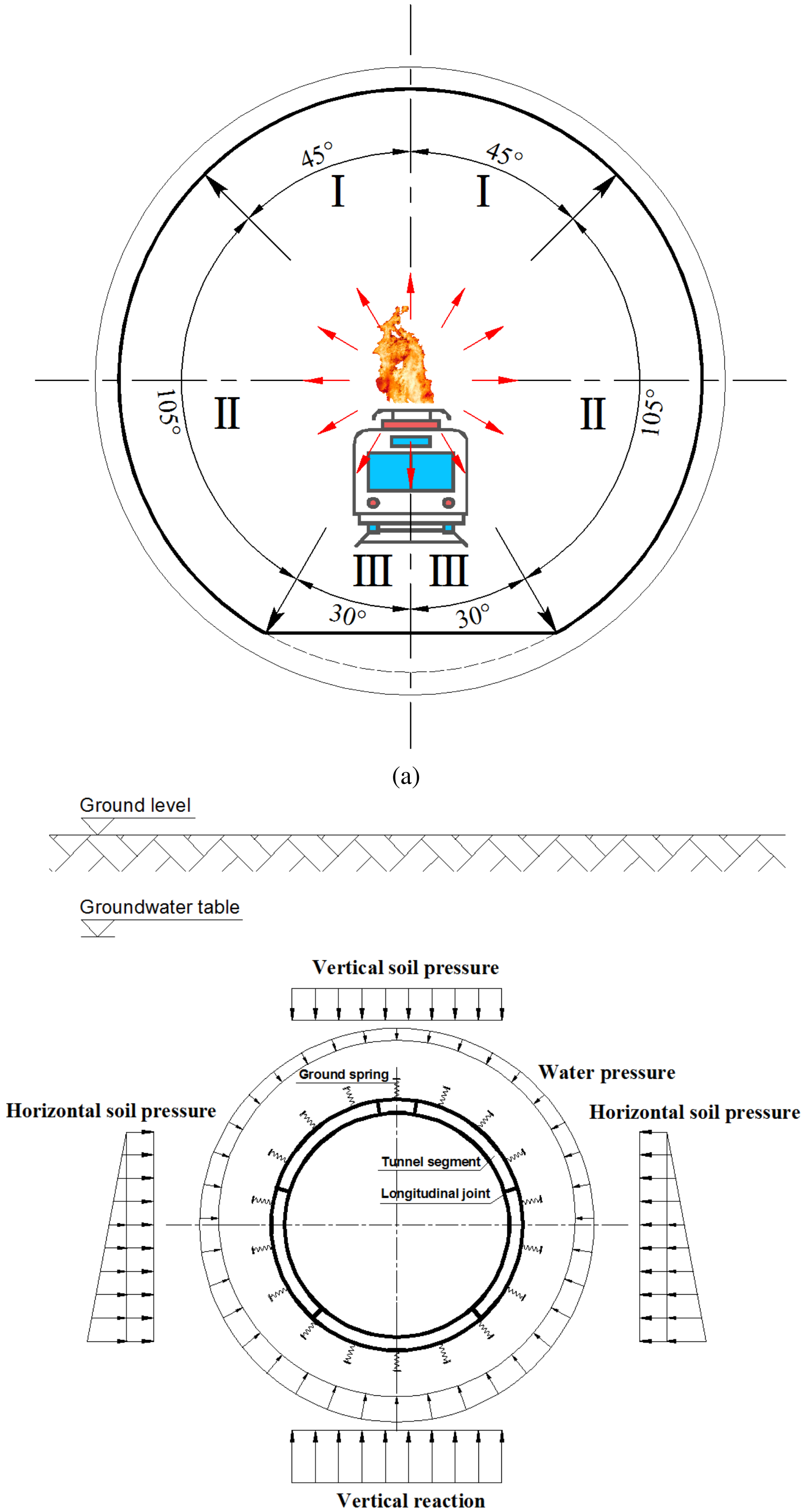

(a) (b)

Fig. 2 Determination of boundary condition: (a) Thermal condition; (b) Loading condition.

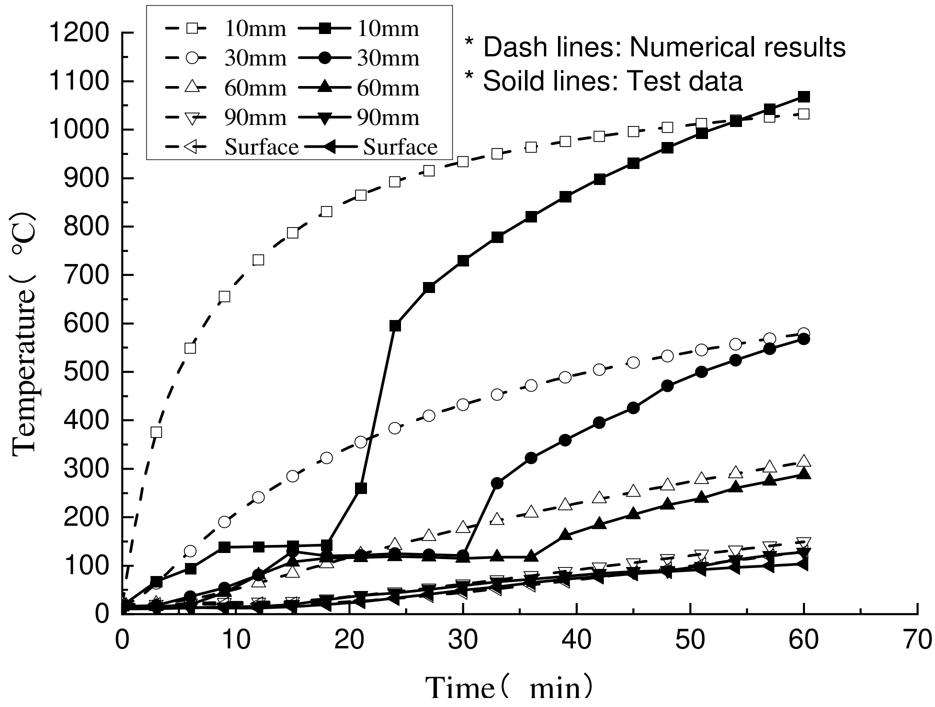

Fig. 3 Comparison of temperature vs. time results between numerical calculation and fire test.

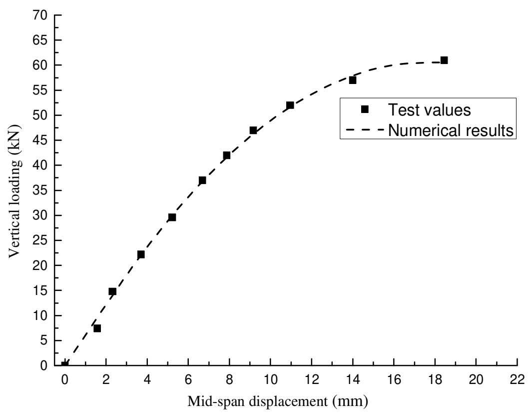

(a)

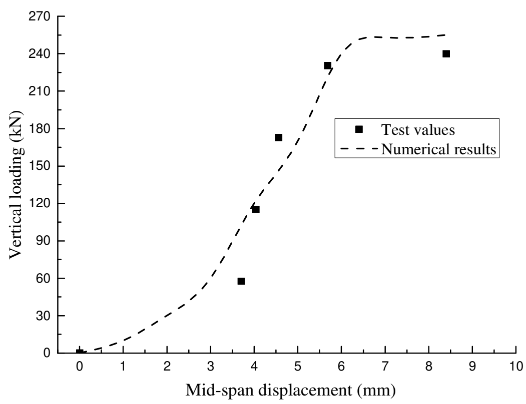

(b)

Fig. 4 Comparison of vertical load vs. mid-span displacement relationships between numerical results and test data: (a) Under sagging moment; (b) Under hogging moment.

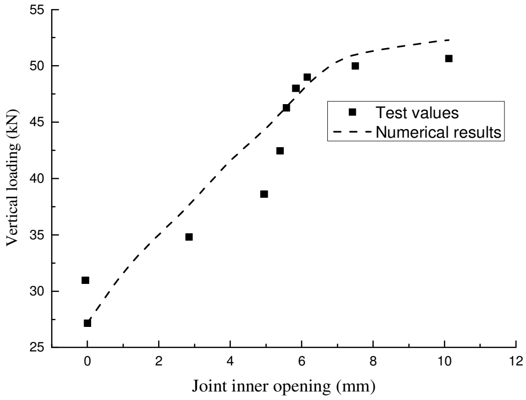

(a)

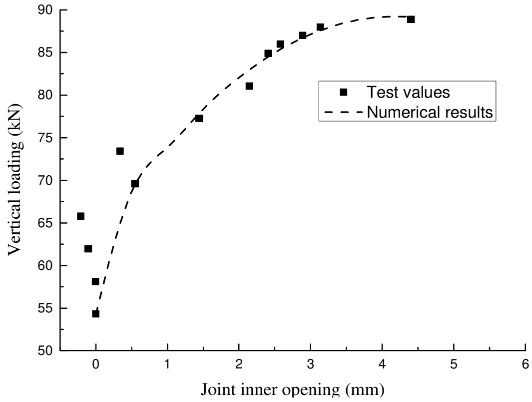

(b)

Fig. 5 Comparison of vertical load vs. joint inner opening relationships between numerical results and test data: (a) Horizontal load = 20kN; (b) Horizontal load = 40kN.

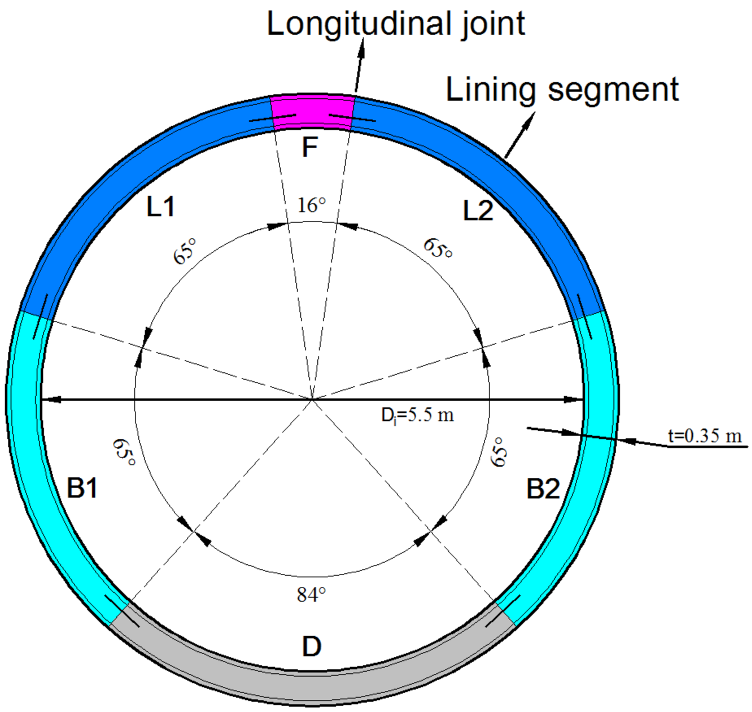

Fig. 6 Layout of a typical segmental ring.

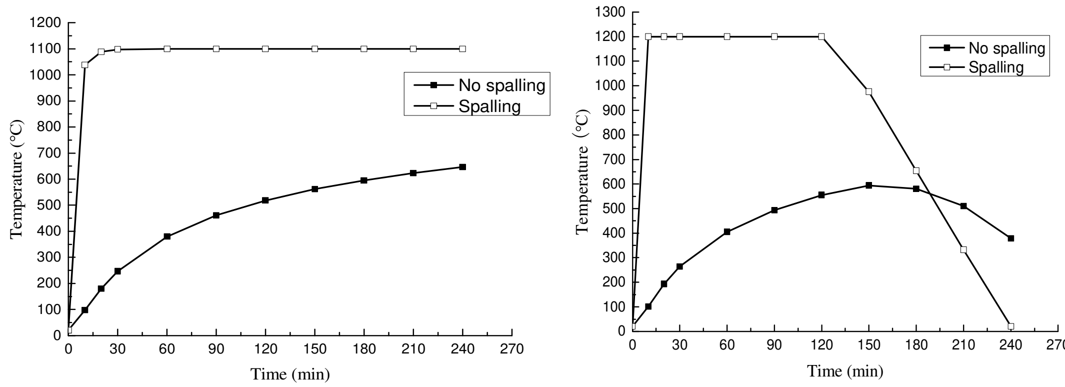

(a) (b)

Fig. 7 Temperature of F segment inner reinforcement vs. time: (a) HC; (b) RABT

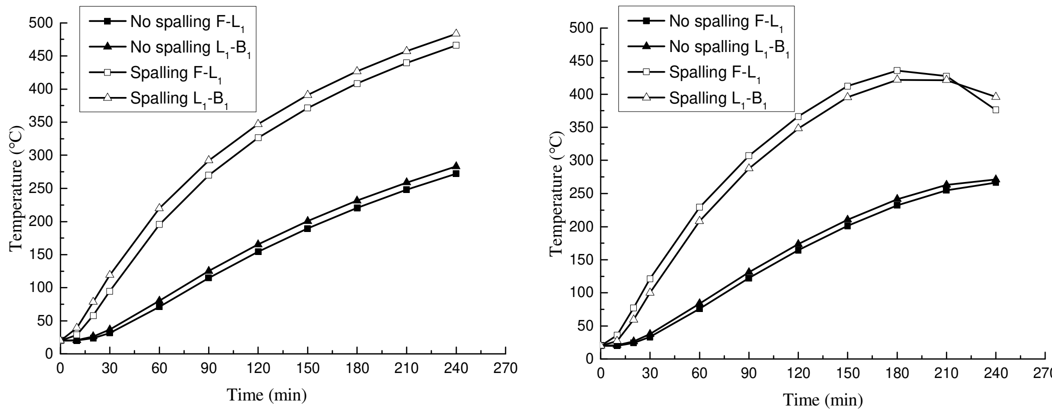

(a) (b)

Fig. 8 Temperature of F-L_1 and L_1-D_1 joint bolts vs time: (a) HC; (b) RABT.

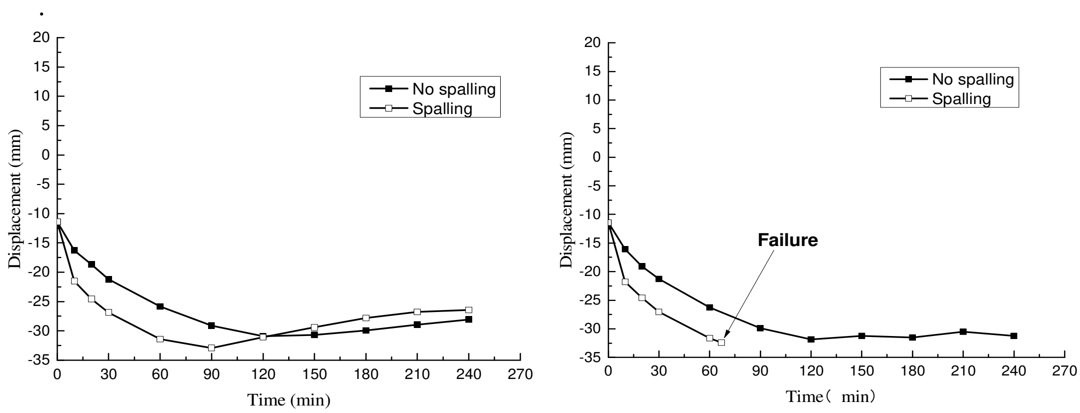

(a) (b)

Fig. 9 Vault vertical displacement vs. time of deep buried tunnel: (a) HC; (b) RABT.

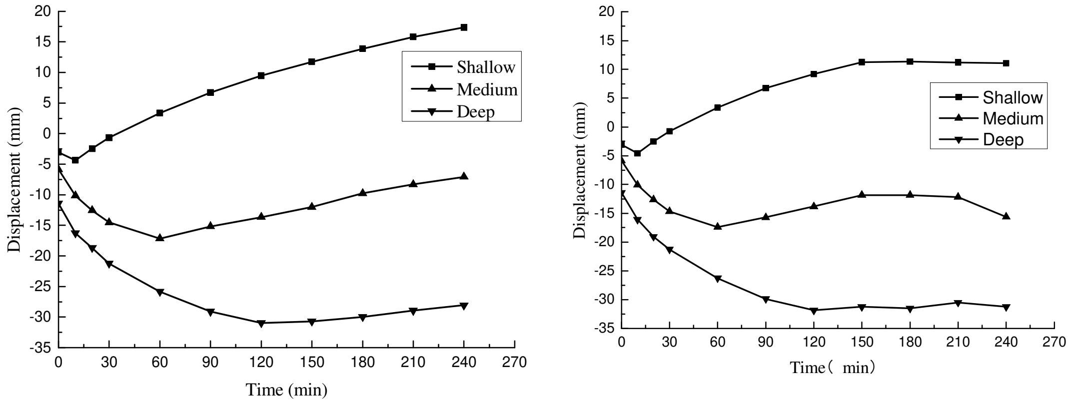

(a) (b)

Fig. 10 Vault vertical displacement vs. time of tunnels in different buried depths: (a) HC; (b) RABT.

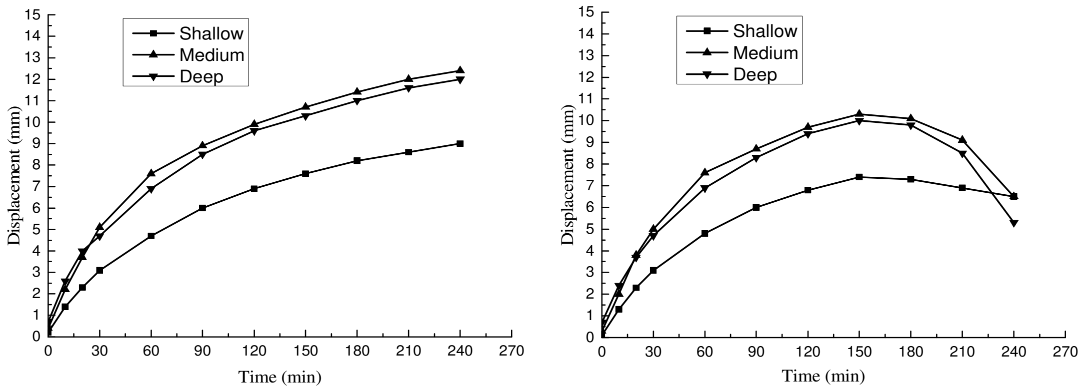

(a) (b)

Fig. 11 L1-B1 joint opening vs. time of tunnels in different buried depths: (a) HC; (b) RABT.

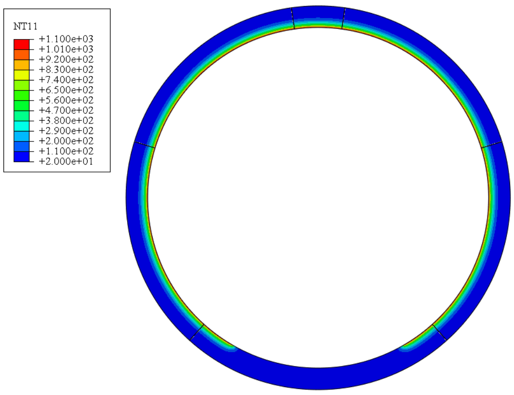

(a)

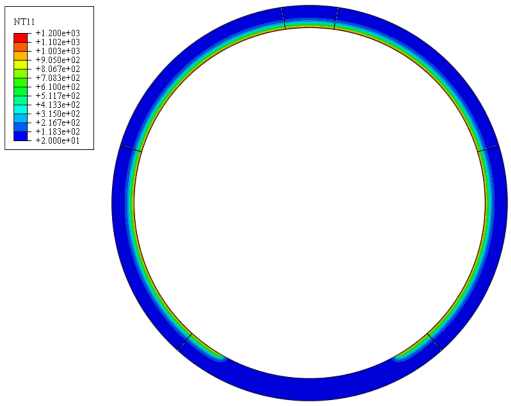

(b)

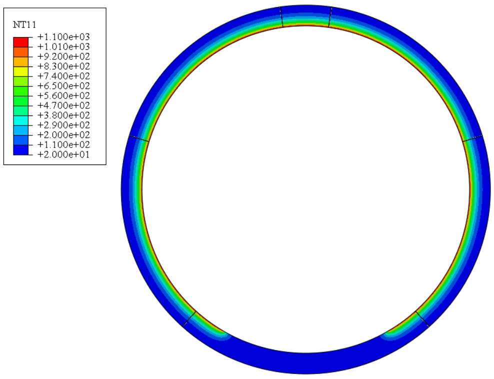

(c)

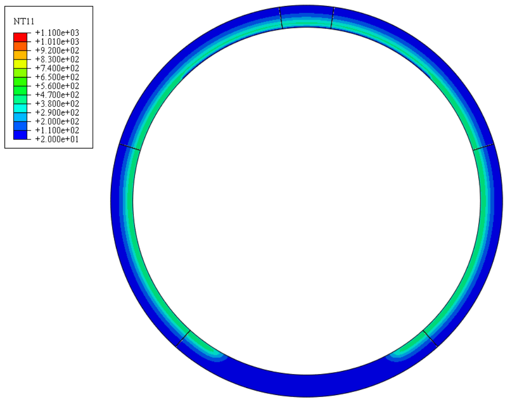

(d)

Fig. 12 Temperature distribution of tunnel: (a) HC-120min; (b) RABT-120min; (c) HC-240min; (d) RABT-240min.

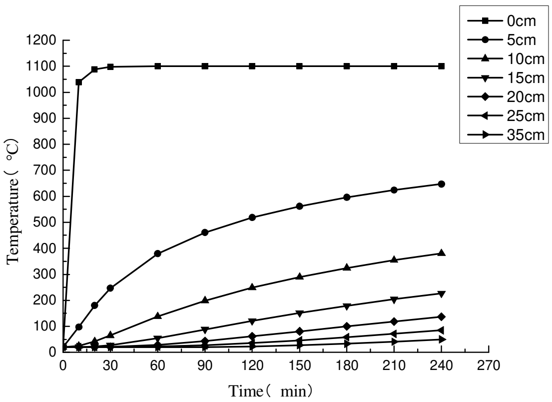

(a)

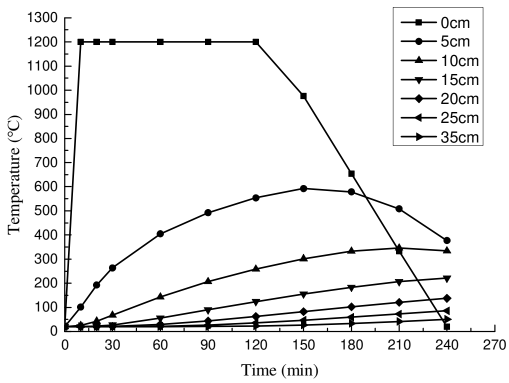

(b)

Fig. 13 Temperature distribution along the thickness of tunnel lining in vault: (a) HC: (b) RABT.

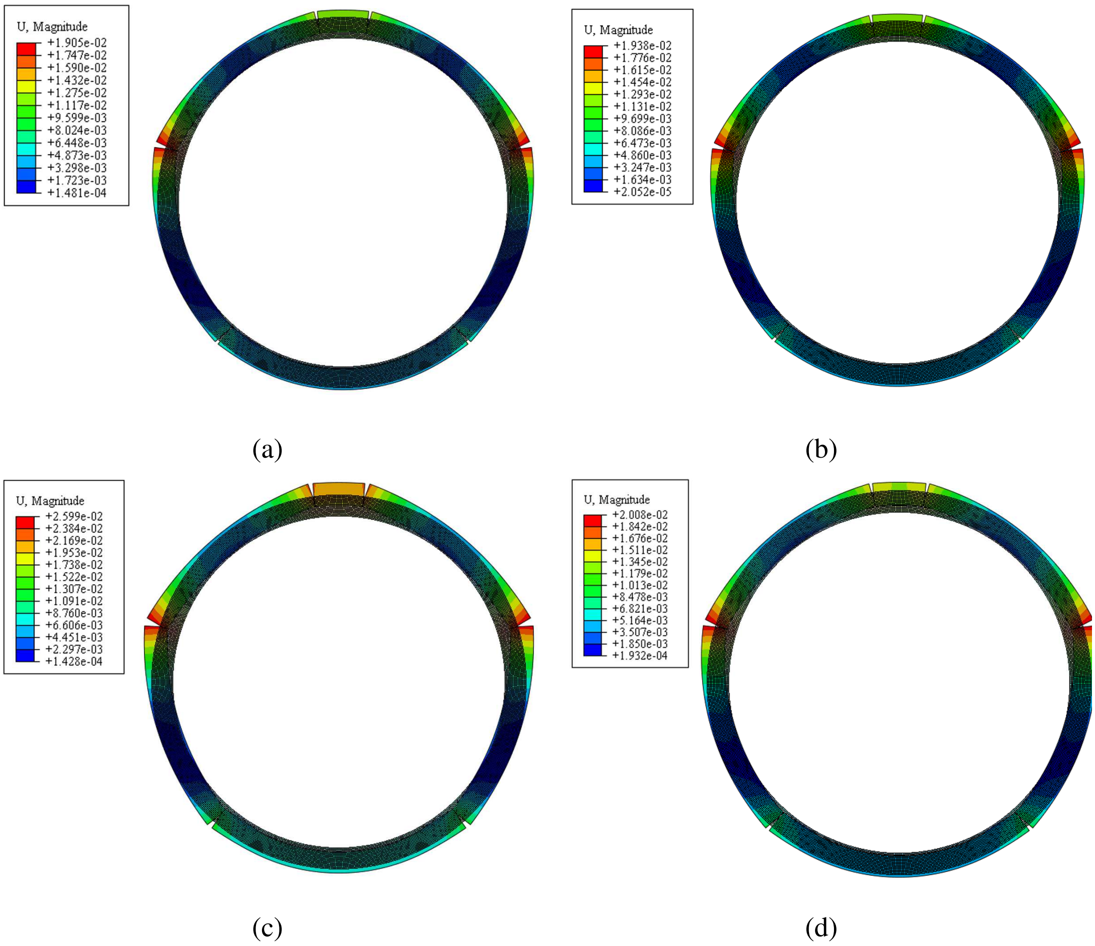

Fig. 14 Deformation of shallow buried tunnel: (a) HC-120min; (b) RABT-120min; (c) HC-240min; (d) RABT-240min.

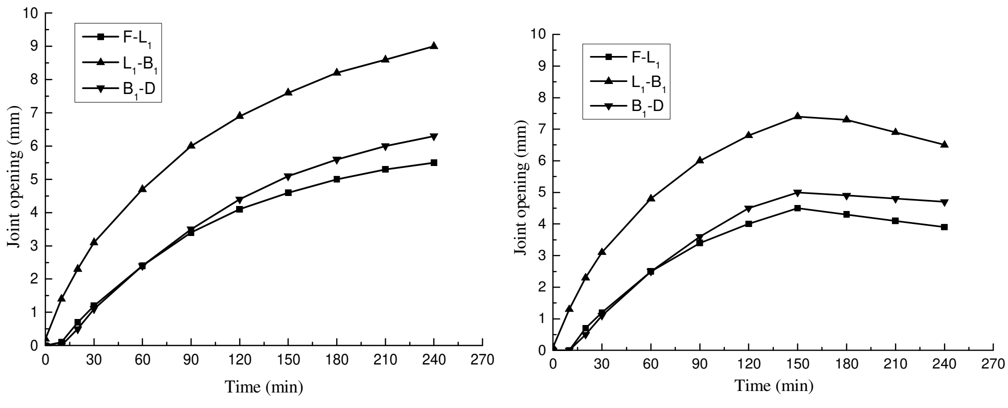

(a) (b)

Fig. 15 Joint opening in shallow tunnel vs, fire duration: (a) HC; (b) RABT.

Appendix A

Table A1 Main thermal and mechanical properties of the segment concrete and steel adopted in the analysis

Type	Unit	Concrete	Steel
Density	kg/m³	2400	7800
Specific heat	J/(kg·°C)	$c_c=\begin{cases}900+80\left(\frac{T}{120}\right)-4\left(\frac{T}{120}\right)^2 & 20^{\circ}\mathrm{C}\le T\le 100^{\circ}\mathrm{C}\\ 900+(T-100) & 100^{\circ}\mathrm{C}\le T\le 200^{\circ}\mathrm{C}\\ 1000+(T-200)/2 & 200^{\circ}\mathrm{C}\le T\le 400^{\circ}\mathrm{C}\\ 1100 & 400^{\circ}\mathrm{C}\le T\le 1200^{\circ}\mathrm{C}\end{cases}$	$c_s=\begin{cases}426+2.22\times10^{-6}T^3-1.69\times10^{-3}T^2+7.73\times10^{-1}T & 20^{\circ}\mathrm{C}\le T\le 600^{\circ}\mathrm{C}\\ 13002/(738-T)+666 & 600^{\circ}\mathrm{C}\le T\le 735^{\circ}\mathrm{C}\\ 17820/(T-731)+545 & 735^{\circ}\mathrm{C}\le T\le 900^{\circ}\mathrm{C}\\ 650 & 900^{\circ}\mathrm{C}\le T\le 1200^{\circ}\mathrm{C}\end{cases}$
Thermal conductivity	W/(m·°C)	$\lambda_c=2-0.2451\frac{T}{100}+0.0107\left(\frac{T}{120}\right)^2 \quad 20^{\circ}\mathrm{C}\le T\le 1200^{\circ}\mathrm{C}$	$\lambda_s=\begin{cases}-3.33\times10^{-2}T+54 & 20^{\circ}\mathrm{C}\le T\le 800^{\circ}\mathrm{C}\\ 27.3 & T\ge 800^{\circ}\mathrm{C}\end{cases}$
Thermal expansivity	-	$\Delta l_c/l_c=\begin{cases}-1.8\times10^{-4}+9\times10^{-6}T+2.3\times10^{-11}T^3 & 20^{\circ}\mathrm{C}\le T\le 700^{\circ}\mathrm{C}\\ 14\times10^{-3} & 700^{\circ}\mathrm{C}\le T\le 1200^{\circ}\mathrm{C}\end{cases}$	$\Delta l_s/l_s=\begin{cases}-2.416\times10^{-4}+1.2\times10^{-5}T+0.4\times10^{-8}T^2 & 20^{\circ}\mathrm{C}\le T\le 750^{\circ}\mathrm{C}\\ 11\times10^{-3} & 750^{\circ}\mathrm{C}\le T\le 860^{\circ}\mathrm{C}\\ -6.2\times10^{-3}+2\times10^{-5}T & 860^{\circ}\mathrm{C}\le T\le 1200^{\circ}\mathrm{C}\end{cases}$
Reduction factor for compressive strength	-	see **Fig. A.1**	see **Fig. A.2**
Reduction factor for tensile strength	-	$\gamma_t(T)=\begin{cases}1.0 & T\le 100^{\circ}\mathrm{C}\\ 1.0-\frac{T-100}{500} & 100^{\circ}\mathrm{C}<T\le 600^{\circ}\mathrm{C}\\ 0 & T>600^{\circ}\mathrm{C}\end{cases}$	see **Fig. A.2**
Reduction factor for tensile strength	-	see **Fig. A.1**	see **Fig. A.2**
Poisson ratio	-	0.2	0.3

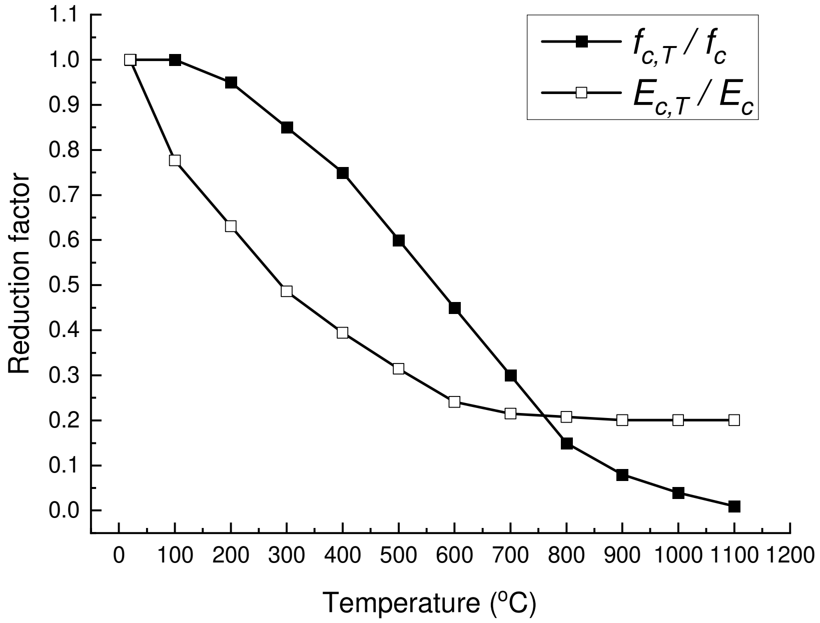

Fig. A.1 Reduction factor of compressive strength (f_c) and elastic modulus (E_c) of concrete at elevated temperatures

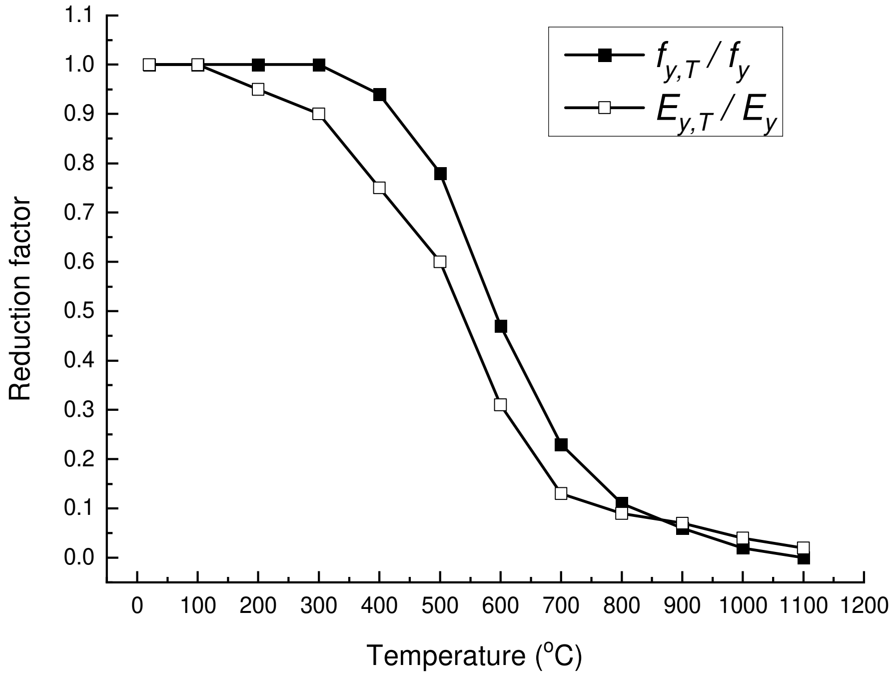

Fig. A.2 Reduction factor allowing for decrease of compressive strength (f_y) and elastic modulus (E_y) of concrete at elevated temperatures